NATIONAL ADVISORY COMMITTEE FOR AERONAUTICS

TECHNICAL NOTE 2854

AVERAGE SKIN-FRICTION DRAG COEFFICIENTS FROM TANK TESTS OF A PARABOLIC BODY OF REVOLUTION (NACA RM-10)

By Elmo J. Mottard and J. Dan Loposer

Langley Aeronautical Laboratory
Langley Field, Va.

Washington
January 1953

NATIONAL ADVISORY COMMITTEE FOR AERONAUTICS

TECHNICAL NOTE 2854

AVERAGE SKIN-FRICTION DRAG COEFFICIENTS FROM TANK TESTS OF A PARABOLIC BODY OF REVOLUTION (NACA RM-10)

By Elmo J. Mottard and J. Dan Loposer

SUMMARY

Average skin-friction drag coefficients were obtained from boundary-layer total-pressure measurements on a parabolic body of revolution (NACA RM-10, basic fineness ratio 15) in water at Reynolds numbers from 4.4×10^6 to 70×10^6. The tests were made in the Langley tank no. 1 with the body sting-mounted at a depth of two maximum body diameters. The arithmetic mean of three drag measurements taken around the body was in good agreement with flat-plate results, but, apparently because of the slight surface wave caused by the body, the distribution of the boundary layer around the body was not uniform over part of the Reynolds number range.

INTRODUCTION

Skin-friction-drag data obtained at high Reynolds numbers in subsonic flow is, at the present time, confined mainly to the results of tests of flat plates. Skin-friction data obtained at high Reynolds numbers from tank tests of a body of revolution would be useful both hydrodynamically and aerodynamically. Such data would make it possible in many instances to estimate the error incurred by using flat-plate data in calculating the skin-friction drag of curved surfaces, such as ship hulls and submerged bodies. The data could be obtained at Reynolds numbers ordinarily obtained in air with supersonic flow and could therefore be used in conjunction with the results of tests of missiles in the same Reynolds number range in order to help evaluate the effect of Mach number on the skin-friction coefficient.

Because of the need for skin-friction coefficients for a curved body at high Reynolds numbers in subsonic flow, skin-friction coefficients were obtained on a parabolic body of revolution (NACA RM-10, basic fineness ratio 15) in water at Reynolds numbers from 4.4×10^6

to 70×10^6 (4.9 feet per second to 78 feet per second). The skin-friction coefficients were obtained from measurements of the total pressure through the boundary layer by the use of the boundary-layer momentum theorem. Measurements were made at the 69.4-percent station (based on the length of the basic shape) at three radial positions around the model. In the transition range of Reynolds number (from 1.1×10^6 to 8.9×10^6), a dye was injected into the boundary layer and the flow was observed on the upper surface of the model.

SYMBOLS

A	skin area from nose to measuring station, sq ft
C_f	average skin-friction drag coefficient
δ	boundary-layer thickness, ft
Δp	static pressure on body minus static pressure in free stream
g	acceleration due to gravity, 32.2 ft/sec^2
h	depth below water surface, ft
μ	absolute viscosity, slugs/ft-sec
p	static pressure, lb/sq ft
p_T	total pressure inside boundary layer, lb/sq ft
p_{T_δ}	total pressure just outside boundary layer, lb/sq ft
q	free-stream dynamic pressure, lb/sq ft
R	Reynolds number based on axial distance from nose to measuring station
r	radial distance from body axis, ft
r_w	radial distance from body axis to skin, ft
ρ	density, slugs/cu ft
s	distance along surface from nose, ft
t	time, sec

τ_w wall shearing stress, lb/sq ft

$\tau_{w_{av}}$ average wall shearing stress, lb/sq ft

u velocity inside boundary layer, fps

U_δ velocity just outside boundary layer, fps

V free-stream velocity, fps

x axial distance from nose, ft

y distance normal to skin, ft

Subscript:

max maximum value

ANALYSIS

Average skin-friction drag coefficients were obtained from rake surveys of the total pressure through the boundary layer and calculated values of the pressure distribution. The average skin-friction coefficient ahead of a measurement station is

$$C_f = \frac{\tau_{w_{av}}}{q} = \frac{2\pi}{qA}\int_0^x \tau_w r_w \, dx \tag{1}$$

Momentum theory is used to evaluate the integral $\int_0^x \tau_w r_w \, dx$ from which the average skin-friction coefficient is obtained. The momentum equation for the boundary layer on the surface of a body of revolution is, from reference 1,

$$\int_0^\delta \rho r \frac{\partial u}{\partial t} dy + \frac{\partial}{\partial s}\int_0^\delta \rho r u^2 dy - U_\delta \frac{\partial}{\partial s}\int_0^\delta \rho r u \, dy = -\frac{\partial p}{\partial s}\int_0^\delta r \, dy - \mu r_w \left(\frac{\partial u}{\partial y}\right)_{y=0} \tag{2}$$

The last term of the equation may be replaced by $\tau_w r_w$, inasmuch as $\mu\left(\frac{\partial u}{\partial y}\right)_{y=0}$ is the shearing stress at the wall. For steady flow, the first term drops out; for incompressible flow, the density ρ is constant. If the body is assumed to be moving at sufficient depth below the surface so that the effect of the surface on the flow is negligible

$$-\frac{\partial p}{\partial s} = \rho U_\delta \frac{dU_\delta}{ds} \tag{3}$$

Using equation (3) and the formula for differentiating a product gives

$$-\frac{\partial p}{\partial s}\int_0^\delta r\,dy = \rho \frac{d}{ds}\int_0^\delta U_\delta{}^2 r\,dy - \rho U_\delta \frac{d}{ds}\int_0^\delta U_\delta r\,dy$$

Equation (2) may then be written

$$\tau_w r_w = \rho \frac{d}{ds}\int_0^\delta \left(U_\delta{}^2 - u^2\right)r\,dy - \rho U_\delta \frac{d}{ds}\int_0^\delta (U_\delta - u)r\,dy \tag{4}$$

For a slender body such as the NACA RM-10, negligible error is introduced by assuming $ds = dx$ and $r = r_w + y$. Making these substitutions, using the formula for differentiating a product, and integrating with respect to x gives:

$$\int_0^x \tau_w r_w\,dx = \rho r_w U_\delta{}^2 \int_0^\delta \left(\frac{u}{U_\delta} - \frac{u^2}{U_\delta{}^2}\right)dy + \rho U_\delta{}^2 \int_0^\delta \left(\frac{u}{U_\delta} - \frac{u^2}{U_\delta{}^2}\right)y\,dy +$$

$$\rho \int_0^x \left[\frac{dU_\delta}{dx} r_w U_\delta \int_0^\delta \left(1 - \frac{u}{U_\delta}\right)dy\right]dx +$$

$$\rho \int_0^x \left[\frac{dU_\delta}{dx} U_\delta \int_0^\delta \left(1 - \frac{u}{U_\delta}\right)y\,dy\right]dx \tag{5}$$

Evaluation of the first and second integrals on the right-hand side of equation (5) requires that the velocities through and just outside the boundary layer be known. These velocities were obtained from measurements of the total pressures. The relation between the pressures and velocities is given by

$$\left.\begin{aligned} \tfrac{1}{2}\rho u^2 &= p_T - \rho g h - \frac{\Delta p}{q}\frac{\rho V^2}{2} \\ \tfrac{1}{2}\rho U_\delta{}^2 &= p_{T_\delta} - \rho g h - \frac{\Delta p}{q}\frac{\rho V^2}{2} \end{aligned}\right\} \qquad (6)$$

where Δp is the static pressure on the body minus the static pressure in the free stream. The value of $\Delta p/q$ at the measurement station was obtained from reference 2, which gives the calculated pressure distribution for the NACA RM-10 body shape in an incompressible fluid of infinite extent.

The first and second terms on the right-hand side of equation (5) represent the total momentum loss in the boundary layer as measured by the rake. The third and fourth terms on the right-hand side account for the momentum change in the boundary layer due to pressure gradient. A linear variation of $\int_0^\delta \left(1 - \frac{u}{U_\delta}\right)dy$ with x was assumed in order to evaluate the importance of the third term. The third term was found to contribute less than 1 percent of the total and was therefore neglected. The fourth term was likewise neglected since it contributed even less than did the third term.

In the computations made in order to obtain the skin-friction coefficients, equations (6) were used to evaluate the terms on the right-hand side of equation (5), which was integrated graphically in order to obtain the value of $\int_0^x \tau_w r_w \, dx$ required for the solution of equation (1).

MODEL AND APPARATUS

The tests discussed herein were made in the Langley tank no. 1 which is described in reference 3. The model and towing support are shown in figures 1 and 2.

The model was spun in sections from 2S aluminum and assembled with flush rivets. The surface was polished after assembly. During the course of the tests, the surface roughness was of the order of 25 micro-inches root mean square. The model was supported from the carriage at a depth at the center line of 2 feet below the water surface.

The towing support was a welded framework of hollow steel struts, 12 percent thick, welded to a steel pipe which extended into the model. The strut section was selected because of its high incipient cavitation speed. The towing support was connected to the towing carriage by a welded framework of steel tubing. The model was electrically insulated from the towing support to prevent galvanic corrosion.

The total pressures in and just outside the boundary layer were measured by means of three rakes equally spaced around the body, 10.41 feet from the nose. Each rake had six total-pressure tubes, two of which were outside the boundary layer. The supporting strut for the tubes had a circular-arc section with a thickness ratio of 10.7 percent. The configuration of the rakes and their locations on the model are shown in figures 3 and 4. Because of the large range of total pressure measured over the Reynolds number range of the tests, three types of instrumentation were necessary. At the high Reynolds numbers (36×10^6 to 70×10^6), a diaphragm type of recording instrument was used; in the intermediate range of Reynolds number (9.4×10^6 to 45×10^6), a mercury manometer was used; for the low-speed range (4.4×10^6 to 12×10^6), a water manometer was used. In the low-speed range, the height of the wave above the rake station was recorded by wave-measuring devices, one located directly above the center line of the model and one located $13\frac{1}{2}$ inches from the center line. After the rake surveys were completed, two flush orifices were installed 2 inches from the nose from which dye could be ejected for observation of the boundary layer.

PROCEDURE

The data were taken during the constant-speed interval of the test run after the pressures had reached an equilibrium value.

In the low-speed range, the flow was made visible by injecting a thin dye stream into the boundary layer. At Reynolds numbers where the boundary layer was not completely turbulent, initial turbulence in the tank was minimized by scheduling the runs in order of increasing speed and allowing a 25-minute idle period before each run.

The alinement of the model with the direction of motion was checked during the test runs and found to be within $\pm\frac{1}{4}^\circ$.

In order to minimize corrosion of the aluminum skin of the model by the salt water in which it was tested, the model was taken out and washed with fresh water at the end of each day's testing, and was polished before again being put into the water.

RESULTS AND DISCUSSION

Typical velocity profiles are shown in figure 5. The agreement of the results from the two outside tubes shows that they are both outside the boundary layer. The average skin-friction coefficients as obtained by the use of equation (5) at the three radially spaced measurement stations are plotted against Reynolds number in figure 6. An indication of the repeatability of the final results can be obtained by comparing data points from runs made at similar Reynolds numbers.

Included in figure 6 is the Schoenherr line which represents the average value of the skin-friction coefficients from most of the available flat-plate skin-friction data for fully turbulent flow. (Schoenherr's skin-friction formulation is explained in refs. 4 and 5.) The agreement between experimental skin-friction coefficients measured at the three rake stations and those predicted from the Schoenherr line is good at low and high Reynolds numbers. At intermediate Reynolds numbers (corresponding to velocities in the region of the maximum velocity of propagation of waves in the tank at the test water level) the skin-friction coefficients differ for the different rakes with an apparent increase in skin-friction coefficient with an increase in depth at the measuring station. Such a trend would occur if the entire boundary layer were being swept downward by a very slight vertical component of flow, such as might exist if the surface distrubance which accompanied the model had its trough located above the measuring station. Wave measurements at Reynolds numbers from 4.4×10^6 to 12×10^6 showed that the trough of the wave was indeed located above the rake station. The maximum depression of 1.1 inches at the rake station occurred at a Reynolds number of 8.9×10^6. Apparently, large errors can result from only small amounts of cross flow if only one rake is used on this type of body.

The arithmetic mean of the average skin-friction coefficients from the three rakes is plotted against Reynolds number in figure 7. It is seen from this plot that not only the coefficients at low and high Reynolds numbers agree with those predicted from the Schoenherr line but also the mean of the three rather widely different coefficients obtained at the intermediate Reynolds numbers agrees well with the Schoenherr line value.

At Reynolds numbers low enough for the laminar region on the model to extend aft of the dye orifices, the extent of the laminar region was clearly indicated by the dye stream. The length of the laminar region at various Reynolds numbers is tabulated thus:

Reynolds number, R	Length of laminar region in percent of total length from nose to rake station, $\frac{x}{10.41} \times 100$
1.1×10^6	>100
2.2	86
4.4	27
6.6	4
8.9	<1.6

The data plotted in reference 5 indicate the Reynolds number of transition for flat plates in water to be about 3×10^5. In the present investigation, the flow was observed over the upper surface only and the flow on the bottom may have been different because of the wave accompanying the model; a direct comparison with the flat-plate data, therefore, is not possible.

CONCLUDING REMARKS

For a streamline body of revolution with a basic fineness ratio of approximately 15 (NACA RM-10), the average skin-friction drag coefficient for the forward 69 percent of the basic body in incompressible flow was very nearly the same as that for flat plates.

The distribution of the boundary layer around the body was apparently affected by a very small cross component of flow over part of the Reynolds number range.

Langley Aeronautical Laboratory,
National Advisory Committee for Aeronautics,
Langley Field, Va., October 8, 1952.

REFERENCES

1. Fluid Motion Panel of the Aeronautical Research Committee and Others: Modern Developments in Fluid Dynamics. Vol. I, S. Goldstein, ed., The Clarendon Press (Oxford), 1938, p. 133.

2. Jones, Robert T., and Margolis, Kenneth: Flow Over a Slender Body of Revolution at Supersonic Velocities. NACA TN 1081, 1946.

3. Truscott, Starr: The Enlarged N.A.C.A. Tank, and Some of Its Work. NACA TM 918, 1939.

4. Von Kármán, Th.: Turbulence and Skin Friction. Jour. Aero. Sci., vol. 1, no. 1, Jan. 1934, pp. 1-20.

5. Davidson, Kenneth S. M.: Resistance and Powering. Detailed Considerations - Skin Friction. Vol. II of Principles of Naval Architecture, ch. II, pt. 2, sec. 7, Henry E. Rossell and Lawrence B. Chapman, eds., Soc. Naval Arch. and Marine Eng., 1939, pp. 76-83.

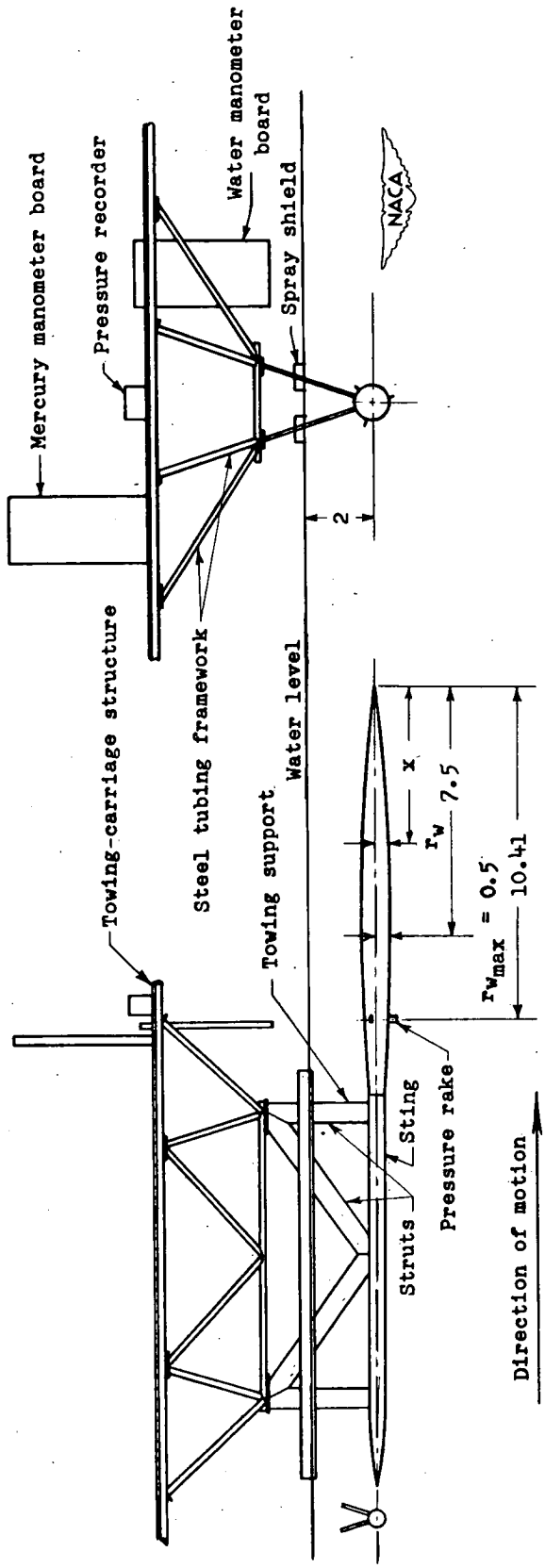

Figure 1.- General arrangement of model and apparatus. (Dimensions are in feet.) Body-profile equation: $r_w = 0.5 - 0.00889(7.5 - x)^2$.

Figure 2.- Model mounted on towing support.

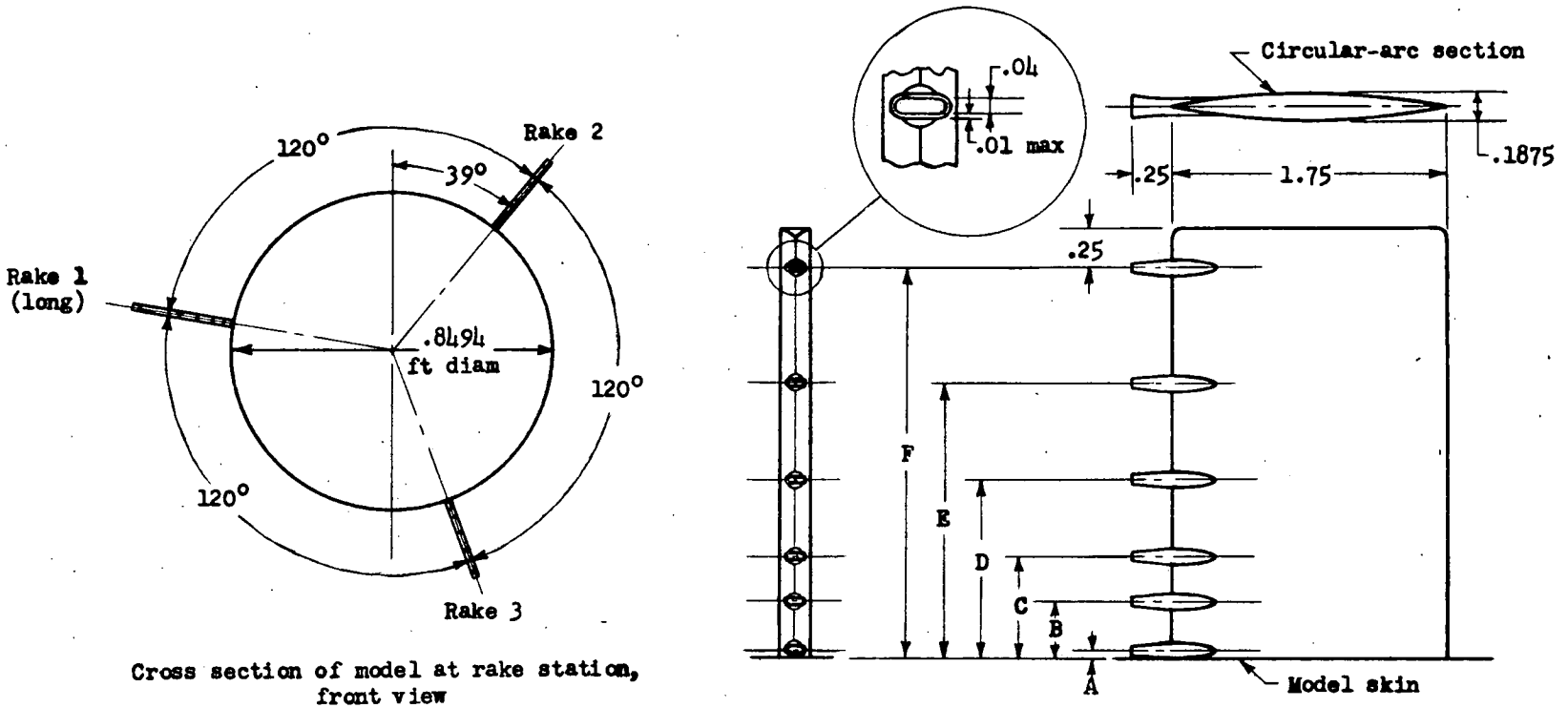

Distance	Rake 1	Rake 2	Rake 3
A	0.055	0.050	0.050
B	.380	.360	.335
C	.675	.655	.630
D	1.170	1.150	1.130
E	1.775	1.760	1.735
F	3.025	2.510	2.480

Figure 3.- Arrangement and configuration of total-pressure rakes.
(Dimensions are in inches except as noted.)

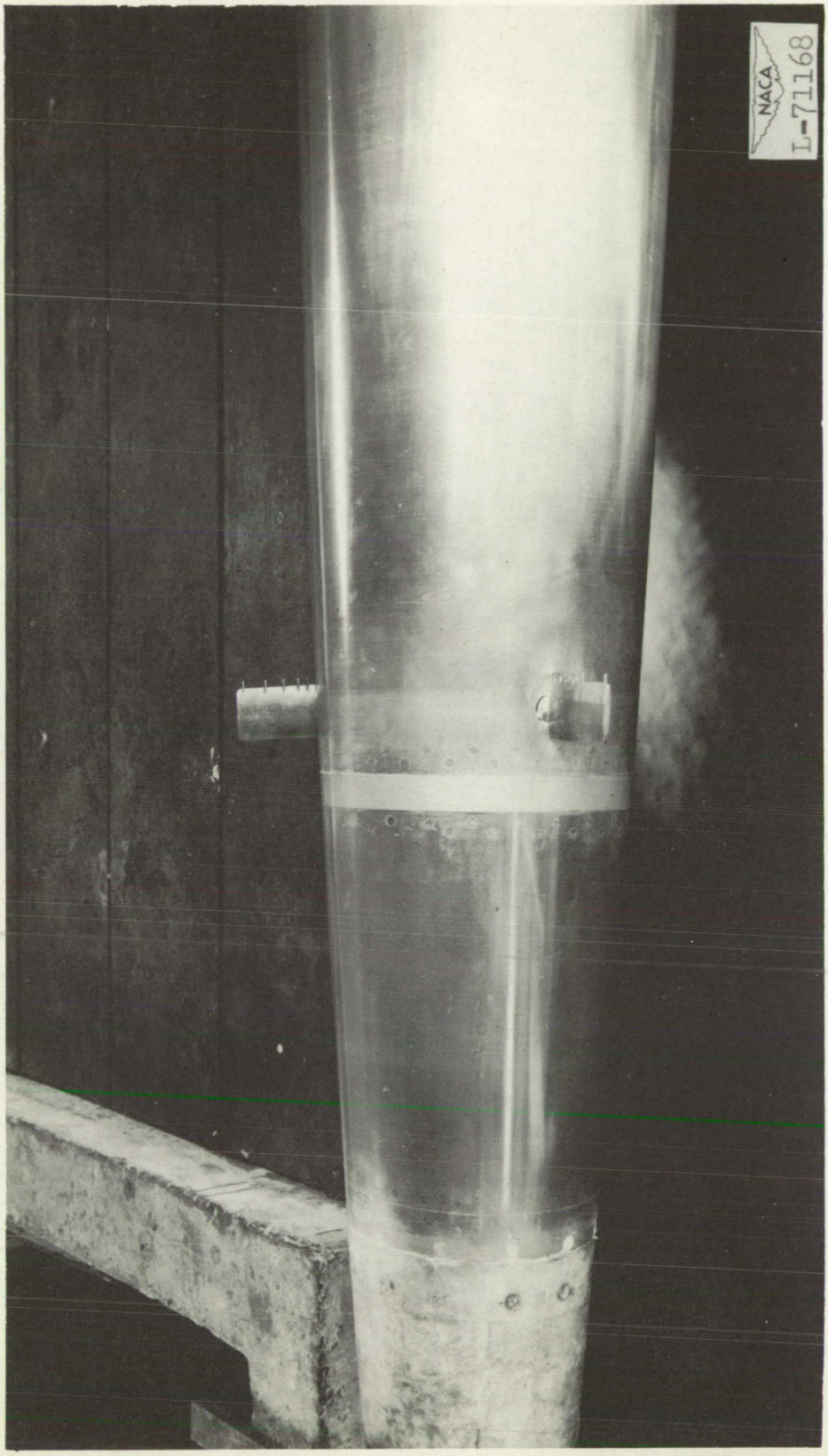

Figure 4.- View of model at rake station.

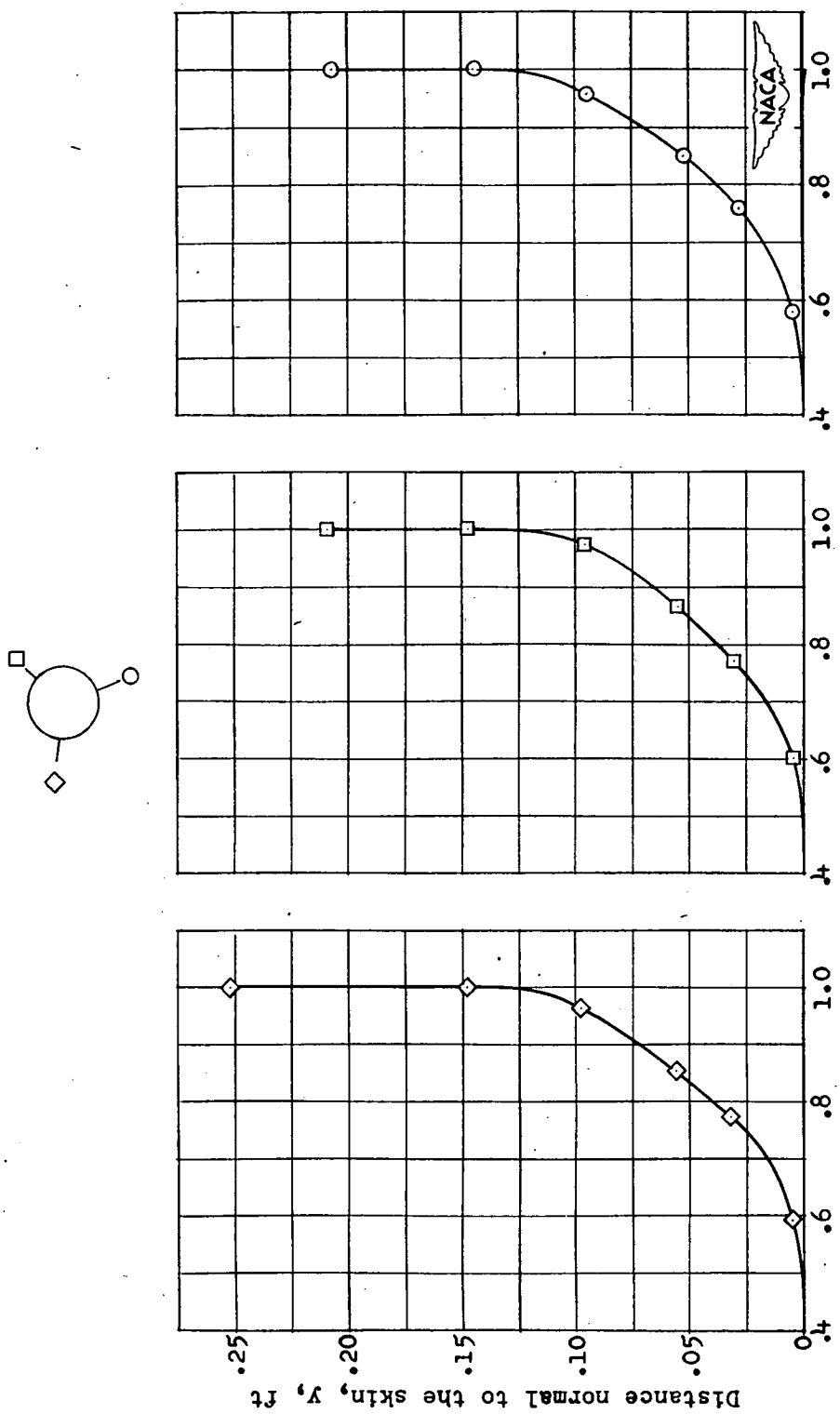

(a) Reynolds number, 4.4×10^6.

Figure 5.- Variation of the nondimensional velocity ratio with distance normal to the skin.

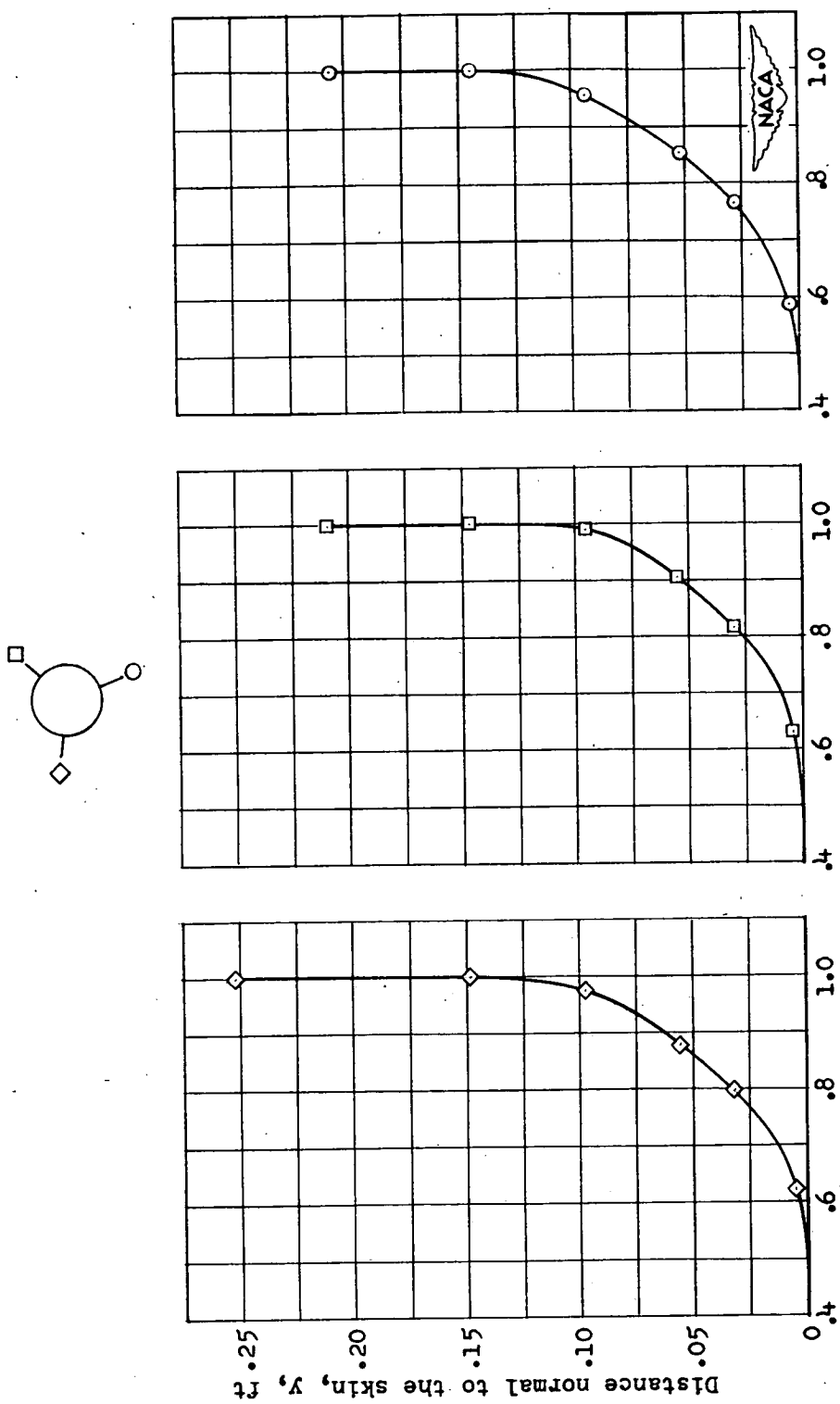

(b) Reynolds number, 8.9×10^6.

Figure 5.- Continued.

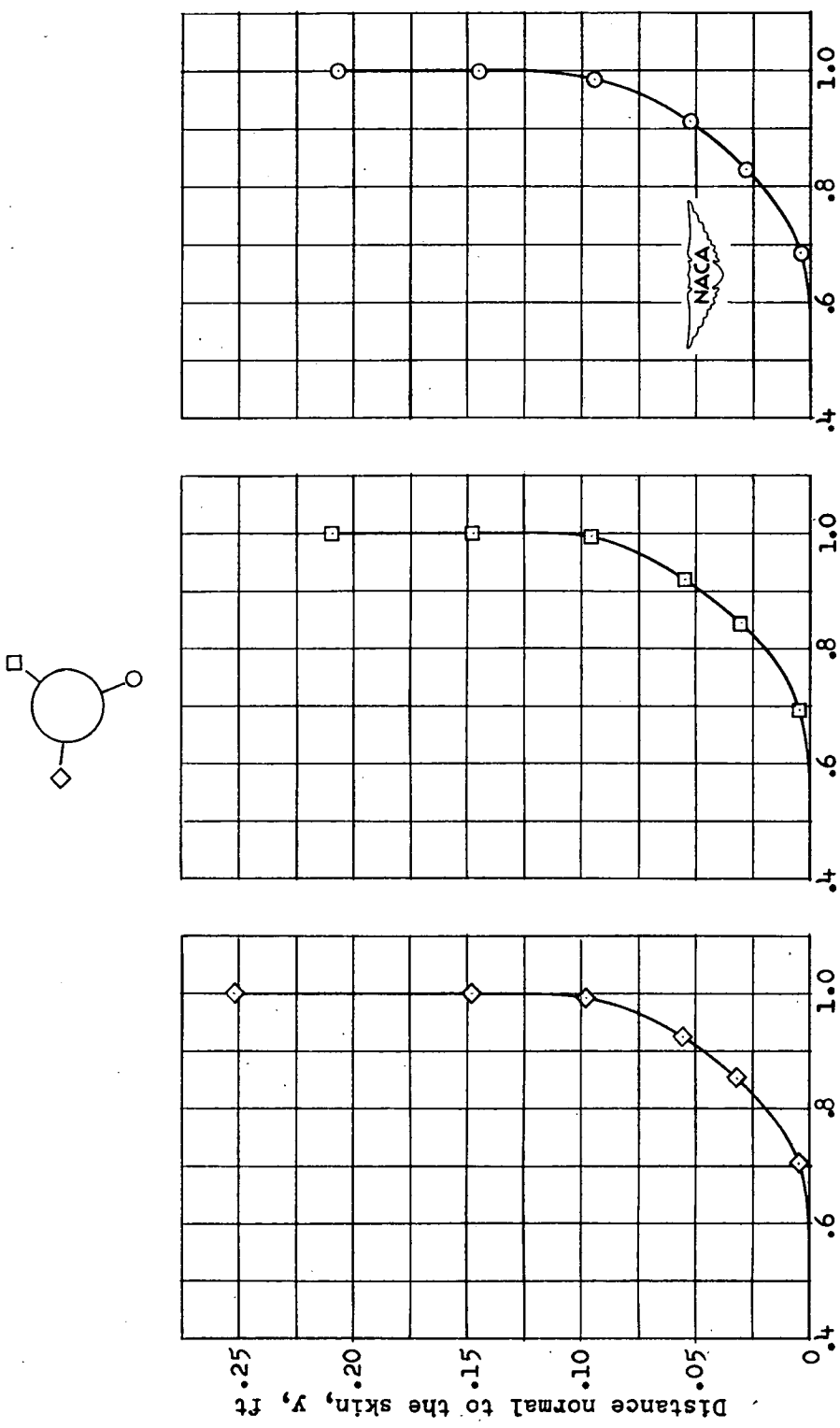

(c) Reynolds number, 69×10^6.

Figure 5.- Concluded.

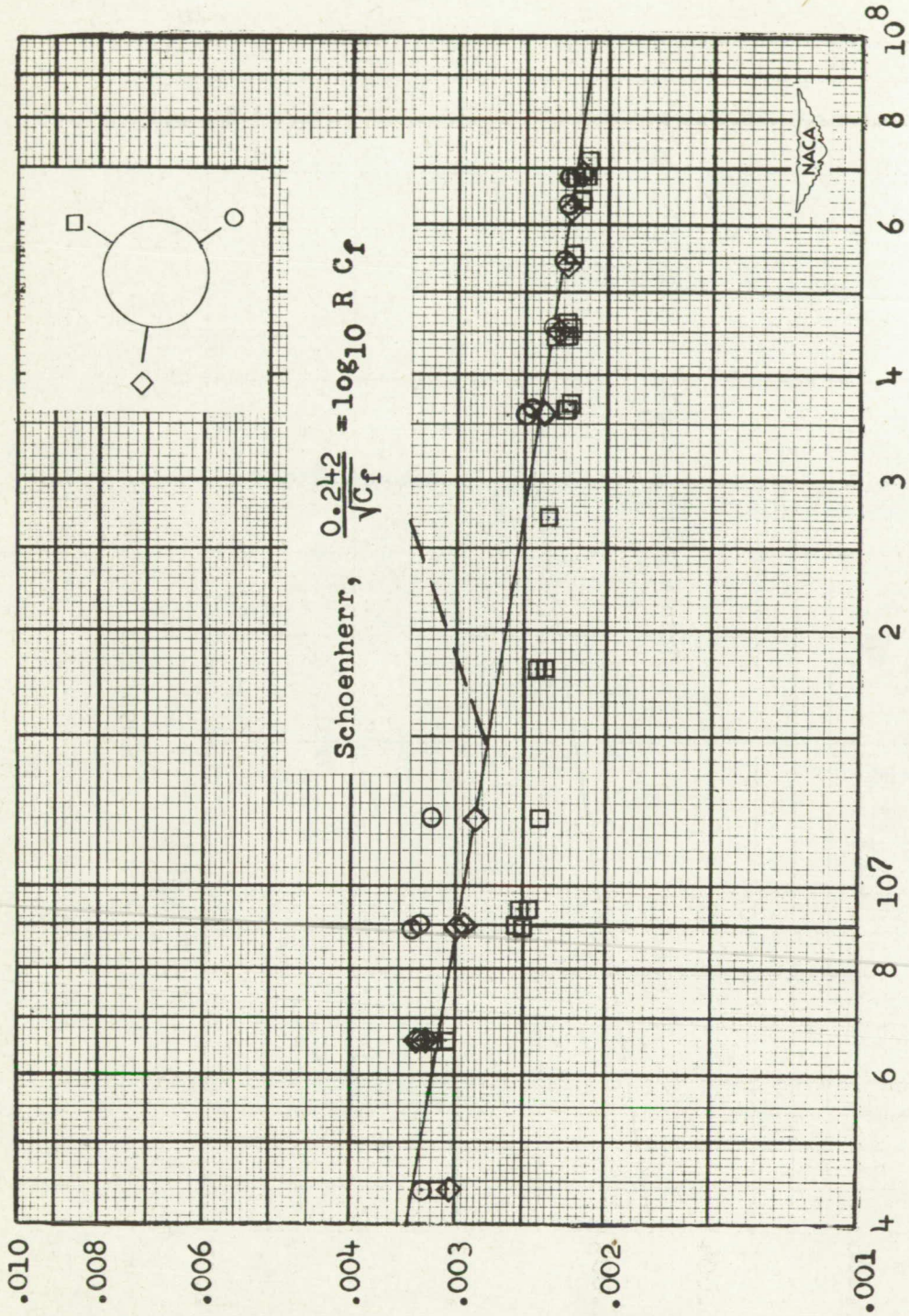

Figure 6.- Variation of average skin-friction coefficient, at the three measurement stations, with Reynolds number.

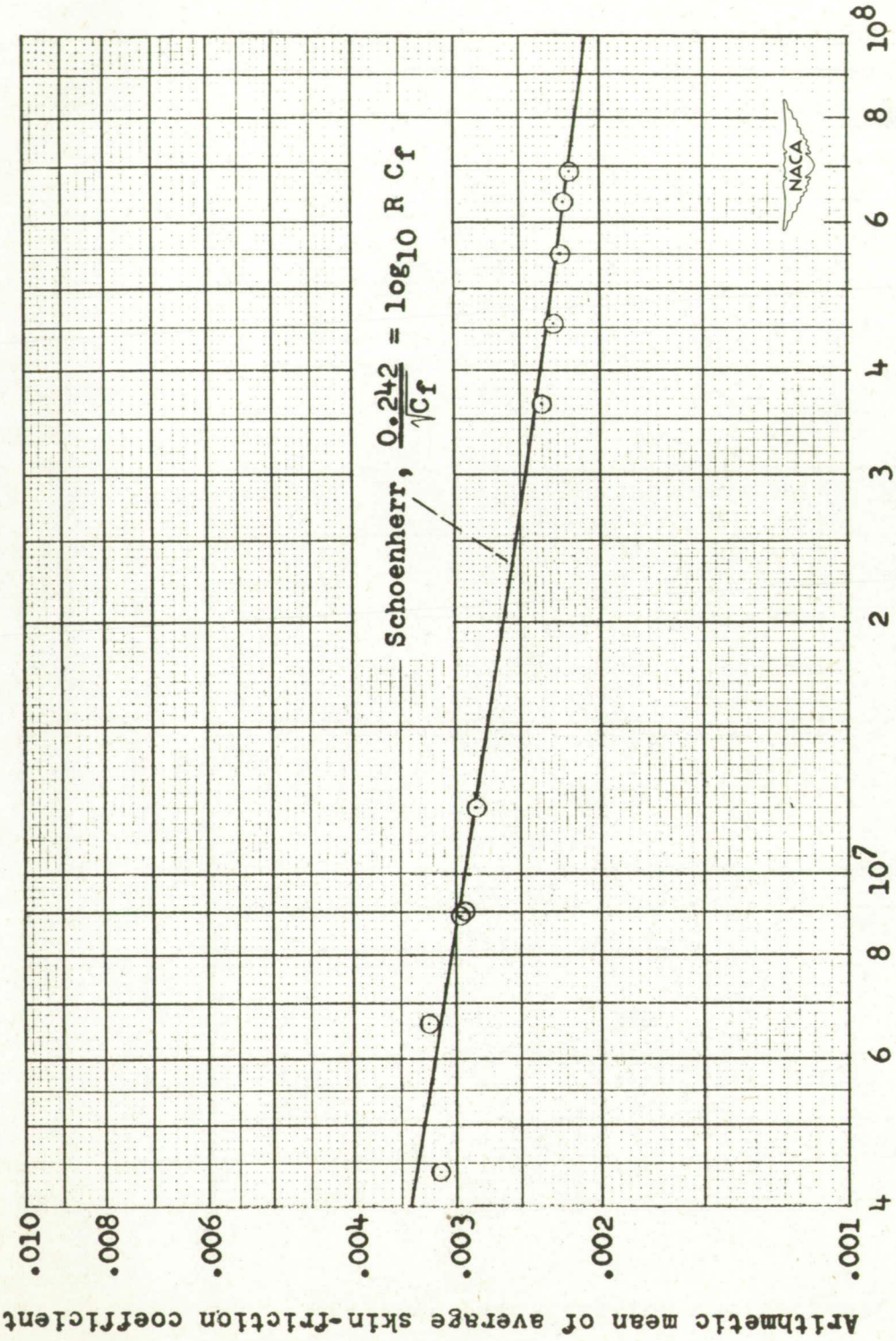

Figure 7.- Variation of arithmetic mean of average skin-friction coefficients with Reynolds number.